A Wideband Metamaterial Meander-Line Antenna

Colan G. M. Ryan and George V. Eleftheriades
Edward S. Rogers, Sr., Department of Electrical and Computer Engineering
University of Toronto
Toronto, Canada
colan.ryan@utoronto.ca

Abstract—**A compact metamaterial meander-line antenna is presented which achieves co-directed currents on the antenna arms. Due to the introduction of an additional resonance, a very wide measured -10 dB return loss bandwidth from 3.5 GHz to 6 GHz is obtained while maintaining a measured radiation efficiency of 87% or greater.**

Keywords-metamaterial; meander-line antenna; wideband

I. INTRODUCTION

Transmission-line metamaterials were introduced in 2002, (see, for example [1]) and have since been applied to a variety of microwave devices, including filters, couplers, and antennas [2-4]. For the last application in particular, metamaterial components have been used to reduce the size of resonant-type antennas by creating an embedded compact feed network that ensures all the radiating elements are fed in-phase. Here, we present a meander-line antenna with a metamaterial (MTM) unit cell to obtain a very wide bandwidth while maintaining a compact form-factor. The key concept that is introduced is to use the MTM loading to maintain co-directional currents on the arms of the meander-line antenna while introducing additional resonances to improve the bandwidth. Section II describes the geometry of the metamaterial antenna and briefly compares its performance with that of a conventional meander-line antenna. Section III gives the radiation patterns and radiation efficiency of the new design, while concluding remarks are made in Section IV.

II. ANTENNA DESIGN

A. Antenna Layout with Metamaterial Unit Cell

Transmission-line metamaterials rely on loading a standard line with a series capacitor and a shunt inductor; the resulting structure possesses a "backward-wave" band where the direction of the wavefronts is reversed with respect to the power flow. The proposed antenna is shown in Fig. 1(a) with the dimensions as indicated. Fed from a microstrip line on a 10 mil (0.254 mm) Rogers RO3003 substrate (ε_r=3, tanδ=0.0013), the antenna incorporates a single metamaterial unit cell on the lower arm: the interdigitated capacitor synthesizes the series capacitance while the shunt inductor is implemented by the meandered ground plane extension which is connected to the antenna by a via though the substrate. The antenna was simulated in a full-wave simulator and Fig. 1(b) shows the simulated current flow on the structure at the onset of the operating band at 3.5 GHz. It is observed that in-phase currents are established on both arms. For comparison, a meander-line antenna without the metamaterial unit cell has also been designed and simulated over the same frequency range. Fig. 1(c) shows the direction of the current flow on this "right-handed" antenna where it is clear that no reversal of the current direction occurs and so the currents on each of the arms remain out-of-phase. The added MTM cell affects the currents on Arm 2 and Arm 3 only, thus allowing independent control of the resonant frequencies associated with these arms, as described in the following section.

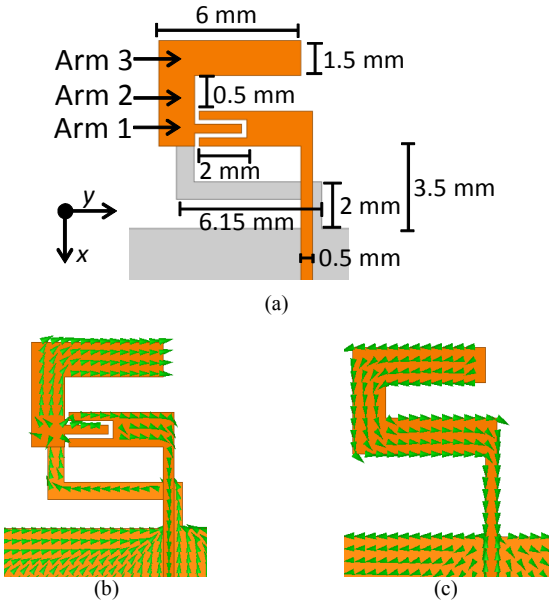

Fig. 1. (a) Geometry of proposed antenna with the ground plane (size: 15 mm x 60 mm) colored light-grey; (b)-(c) surface current direction on metamaterial and conventional meander antennas, respectively.

B. Comparison of Conventional and Metamaterial Meander Antennas

The main benefit of the new antenna is its wide bandwidth as compared to the conventional meander antenna. Fig. 2 compares the simulated return loss versus frequency characteristics for both types of antennas. A significantly wider bandwidth is obtained for the proposed structure: the -10 dB bandwidth extends from 3.5 GHz to 6.5 GHz, whereas the conventional meander antenna has a -10 dB bandwidth from 3.6 GHz to 5 GHz. A key difference is the introduction of an additional high-frequency resonance, occurring at approximately 5.6 GHz, which results in the

bandwidth improvement. The source of this added resonance becomes clear once the current distribution on the metamaterial antenna is examined. Fig. 3 plots the magnitude of the surface current density at each of the resonant frequencies. For the resonance labeled *Mode 1*, Fig. 3(a) shows the current extending over all arms of the antenna. For *Mode 2*, the current is largely confined to Arm 1 and Arm 2 only as seen in Fig. 3(b). Both of these current distributions may also be observed in the right-handed antenna and correspond to the two dips in the return loss curve of Fig. 2. The current for *Mode 3* is concentrated on Arm 1; this distribution is not excited for the conventional antenna and hence, the high-frequency resonance is not observed for that case. It is important to note that the *Mode 1* and *Mode 2* resonant frequencies can be controlled by varying the metamaterial capacitive or inductive loading, rather than by altering the length of Arm 2, as would be the case in a conventional meander antenna.

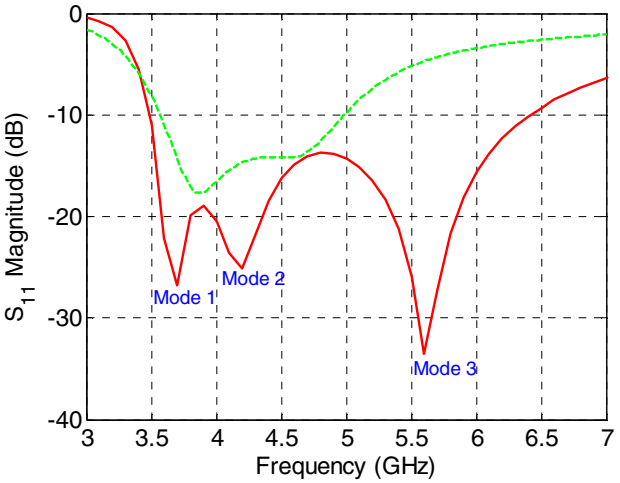

Fig. 2. Return loss for conventional (dashed) and metamaterial (solid) antenna.

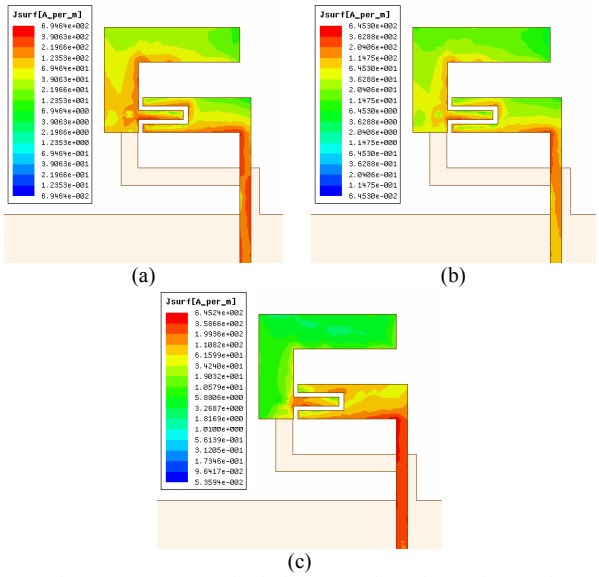

Fig. 3. Current magnitude for (a) Mode 1, (b) Mode 2, and (c) Mode 3.

An additional difference between the metamaterial and conventional meander antenna is the behavior of *Mode 2* as the length of the Arm 2 is varied. As this length is increased in the right-handed antenna, the resonance associated with this mode decreases in frequency; this is expected since the electrical length is now greater. For the metamaterial antenna, however, the opposite result occurs and *Mode 2* shifts upwards. Since the *Mode 1* resonance still shifts down with an increasing overall antenna length, this behavior results in another mechanism by which either the reflection magnitude across the band or the bandwidth itself can be controlled. In the conventional antenna, increasing the spacing between the *Mode 1* and *Mode 2* resonances (and hence, controlling the bandwidth or the reflection magnitude over the band) would require a significantly longer Arm 3. Consequently, this new design offers the additional advantage of a compact size.

III. ANTENNA PERFORMANCE

A. Fabricated Antenna

The constructed metamaterial meander antenna is shown in Fig. 4; it is fed from a coaxial connection through the substrate, and including the ground plane and substrate backing, the total device size is 30 x 60 mm.

B. Measured Results

The measured return loss is shown in Fig. 5 with the simulated data again repeated for comparison. The total measured -10 dB return loss bandwidth is 2.5 GHz and reasonably good agreement between the two sets of data is obtained. The discrepancy in overall magnitude between measured and simulated results is due to the relatively large radius of the coaxial feeding pin; simulations confirm a degradation of matching levels when the inductance of the feed line is decreased as the line itself is widened. For reference, Fig. 6 shows the simulated three-dimensional radiation patterns of the antenna at the *Mode 1* resonance. Fig. 7 and Fig. 8 plot simulated and measured radiation patterns cuts at each of the three resonant frequencies in the *xy* and *xz* planes for horizontal and vertical incident electric fields, respectively. Overall, reasonable agreement is obtained. The measured pattern is tilted in Fig. 8, likely due to a small portion of the coax pin protruding above the surface of the antenna, and so contributing to the radiation pattern. The radiation efficiency (η_{RAD}) of the antenna was measured using the Wheeler cap method [5] and is compared against the simulated efficiency in Table I. The measured efficiency is very high and ranges from 87% to 96% across the band.

Fig. 4. Photograph of fabricated antenna: (a) top layer and (b) bottom layer.

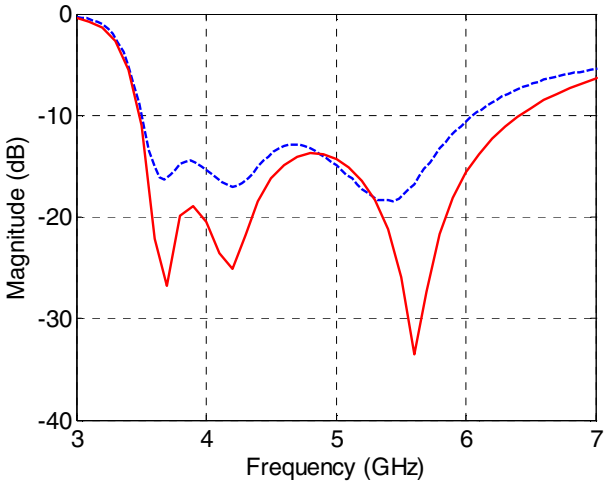

Fig. 5. Comparison of the measured (dashed) and simulated (solid) return loss.

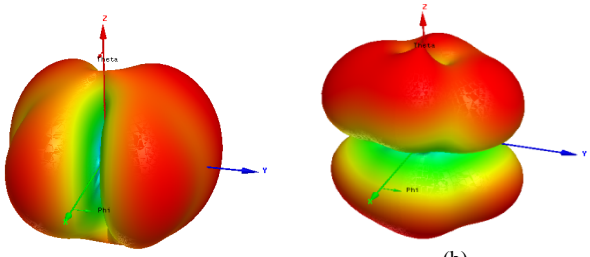

(a) (b)

Fig. 6. (a) GainΦ and (b) Gainθ at 3.7 GHz

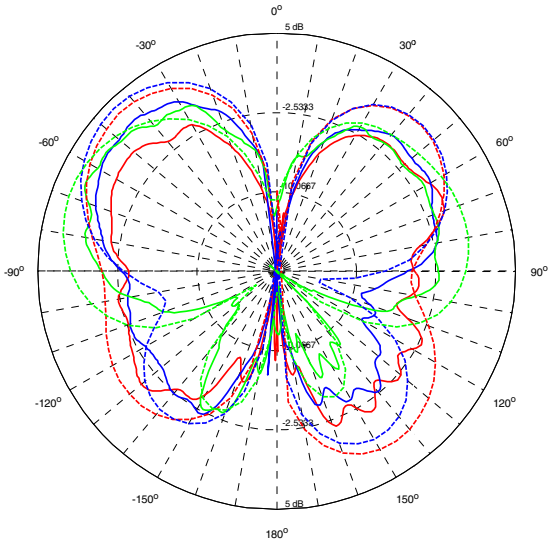

Fig. 7. Measured (solid lines) and simulated (dotted lines) gain in *xy* plane for horizontal incident field at 3.6 GHz (▬), 4.3 GHz (▬), and 5.5 GHz (▬).

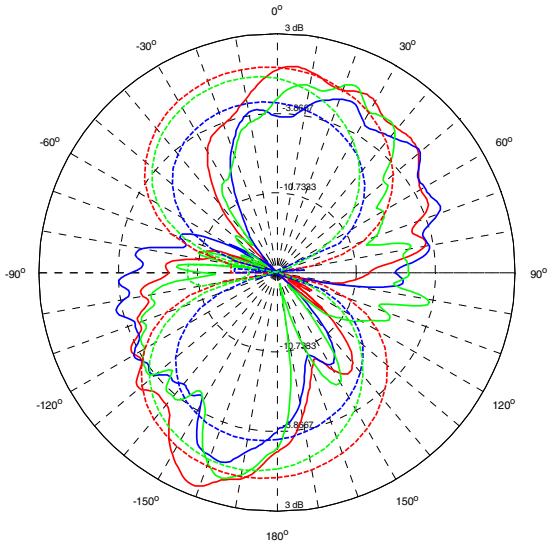

Fig. 8. Measured (solid lines) and simulated (dotted lines) gain in *xz* plane for vertical incident field at 3.6 GHz (▬), 4.3 GHz (▬), and 5.5 GHz (▬).

Frequency (GHz)	η_{RAD} (Simulated)	η_{RAD} (Measured)
3.6	0.97	0.961
4.3	0.98	0.874
5.5	0.99	0.911

IV. CONCLUSIONS

A novel metamaterial meander antenna has been presented which is compact, exhibits both a very wide 2.5 GHz bandwidth and high radiation efficiency, and allows for independent control of the resonant frequencies through the added metamaterial components. The MTM loading results in co-directed antenna currents and also introduces a third resonance which serves to increase the bandwidth over the conventional meander antenna.

REFERENCES

[1] G.V. Eleftheriades, A.K. Iyer, and P.C. Kremer, "Planar negative refractive index media using periodically L-C loaded transmission lines," *IEEE Trans. Microw. Theory Tech.*, vol. 50, pp. 2702-2712, Dec. 2002.

[2] M. Studniberg and G.V. Eleftheriades, "A dual-band bandpass filter based on generalized negative-refractive index transmission-lines," *IEEE Microw. Wireless Compon. Lett.*, vol. 19, no. 1, pp 18-20, Jan. 2009.

[3] M. Duran-Sindreu, G. Siso, J. Bonache, F. Martin, "Planar multi-band microwave components based on the generalised composite right/left handed transmission line concept," *IEEE Trans. Microwave Theory & Tech*, vol. 58, no. 12, pp. 3882-3891, Dec. 2010.

[4] F. Qureshi, M.A. Antoniades, and G.V. Eleftheriades, "A compact and low-profile metamaterial ring antenna with vertical polarization," *IEEE Antennas & Wireless Prop. Letters*, vol. 4, pp. 333-336, Sept. 2005.

[5] H. A. Wheeler, "The radian sphere around a small antenna", *Proc. IRE*, August 1959, pp. 1325-1331.